Tellus
SERIES A DYNAMIC METEOROLOGY AND OCEANOGRAPHY
PUBLISHED BY THE INTERNATIONAL METEOROLOGICAL INSTITUTE IN STOCKHOLM

Tellus (2010), 62A, 361–376

TELLUS

Comparison of three weather prediction models with buoy and aircraft measurements under cyclone conditions in Fram Strait

By ANDREA LAMMERT[1]*, BURGHARD BRÜMMER[1], MICHAEL HALLER[1], GERD MÜLLER[1] and HARALD SCHYBERG[2], [1]*Meteorological Institute, University Hamburg, D-20146 Hamburg, Germany;* [2]*Norwegian Meteorological Institute, Oslo, Norway*

(Manuscript received 23 October 2009; in final form 13 April 2010)

ABSTRACT

Operational model analyses of the European Centre for Medium-Range Weather Forecast (ECMWF), the German Weather Service (DWD) and the Norwegian Meteorological Institute (HIRLAM) are compared to data measured by 16 ice buoys and by a research aircraft in eight flight missions during the Fram Strait cyclone experiment FRAMZY in March/April 2007. The sea level pressure (SLP) compares well with the buoys for all models, SLP correlations are >0.99, SLP tendency correlations are >0.95 and spatial SLP correlations are >0.94 on the average. The aircraft measurements are used for comparison of the horizontal and vertical boundary layer structure in ECMWF and HIRLAM under cyclonic conditions. Horizontal SLP gradients are slightly underestimated. The surface air temperature (SAT) is too low on the warm side and too high on the cold side of the synoptic systems. The temperature inversion on the cold side is not realistically captured with respect to its base and strength in the ECMWF model and with respect to its thickness in HIRLAM. This results in a wrong vertical structure of humidity and wind. The SAT errors hint at model deficits in the representation of the surface energy balance and the inversion errors hint at deficits in the parametrization of the vertical mixing.

1. Introduction

The Fram Strait between Spitsbergen and Greenland is an important region of the North Atlantic climate system. Here, on a narrow distance two ocean currents flow in opposite directions. On the eastern side, the West Spitsbergen Current (WSC) transports warm Atlantic water to the Arctic Ocean. This side is mostly ice-free. On the western side, the East Greenland Current (EGC) transports cold Arctic water to the North Atlantic. The EGC is ice-covered nearly the entire year and about 2700 $km^3\,a^{-1}$ of sea ice are exported from the Arctic Ocean on the long-term average. The ice export varies from year to year (e.g. Häkkinen, 1993; Hilmer et al., 1998; Harder et al., 1998; Kwok and Rothrock, 1999; Häkkinen and Geiger, 2000; Polyakov and Johnson, 2000; Vinje, 2001) but also the various export estimates reported in the literature differ by almost the same order of magnitude as the interannual variations (e.g. Brümmer et al., 2001).

As a consequence of the opposite currents, the Fram Strait is a region with a relatively large atmospheric baroclinicity. This favours cyclogenesis and, thus, the Fram Strait is a region with a high frequency of cyclone occurrence (e.g. Serreze, 1995; Brümmer et al., 2000; Affeld, 2003; Zhang et al., 2004). According to Affeld (2003) there are 4.7 cyclones per month in the area –20°W to 10°E and 76° to 80°N averaged over the period 1978–2000. Cyclones occur only slightly more frequently in winter than in summer, with higher intensity in winter.

The ice export through Fram Strait depends primarily on the atmospheric wind forcing. Large-scale atmospheric circulation patterns play an important role, such as the North Atlantic Oscillation (NAO) (e.g. Hilmer and Jung, 2000), cyclonic and anticyclonic circulation patterns over the Arctic Ocean (Proshutinsky and Johnson, 1997) or the state of the North Atlantic low-pressure zone (Jahnke-Bornemann and Brümmer, 2009). Vinje (2001) found a close relation between the ice export and the sea level pressure (SLP) gradient between 80°N, 10°W and 73°N, 20°E. In a statistical study, Affeld (2003) investigated how the ice export changes when a cyclone is present in the Fram Strait. He related the cyclone tracks determined from the re-analyses (ERA-15) and the analyses of the European Centre for Medium-Range Weather Forecast (ECMWF) to the

*Corresponding author.
e-mail: andrea.lammert@zmaw.de
DOI: 10.1111/j.1600-0870.2010.00460.x

ice export simulated with a coupled ice-ocean model (forced with the ECMWF analyses). The result was a clear cyclone impact on the ice drift: cyclones in the eastern part of the Fram Strait induce an increase of the ice export; in the western part they induce a reduction of the ice export. In another study with an ice model, in which the strength, the propagation speed and the track of cyclones were prescribed, Schröder (2004) demonstrated how sensitive the ice export is with regard to the cyclone track. Tracks, which differ only 100 km in east-west direction, can lead to even opposite signs of the ice export. Thus, a correct analysis of the cyclone and its track is especially important when an ice model is forced with the SLP analysis. But also in a completely coupled ocean–ice–atmosphere model, as for example in a climate model, cyclones must be correctly represented, especially in a key region of the North Atlantic climate system such as the narrow Fram Strait.

There are several challenges for obtaining high quality numerical weather forecasts in the Fram Strait. One issue is the scarcity of conventional routine observations in the surrounding areas. There are some observation stations in Greenland, Iceland and the Norwegian Arctic, but there are large ocean and ice-covered regions nearby where only satellite observations are routinely available. This might affect the quality of the analysis in the operational numerical weather prediction (NWP) data assimilation schemes. Another issue is that most developments and validations of surface and boundary layer parametrizations in NWP systems have been for conditions outside the polar regions. Thus, there might be limitations in the parametrization in the NWP systems of surface and boundary layer processes over sea ice.

Since direct observations of the impact of an individual cyclone on the sea ice and studies on the quality of the cyclone analysis in an operational NWP model did not exist, the first field observations in the Fram Strait with focus on these two topics were conducted during the FRAMZY 1999 (Fram Strait Cyclones) experiment in April 1999 (Brümmer, 2000) and the FRAMZY 2002 experiment in March 2002 (Brümmer et al., 2005a,b, 2008). The FRAMZY 2002 measurements showed that not only cyclones but also fronts have the potential to impact the sea ice significantly. Very narrow surface fronts with strong wind and temperature contrasts were observed (Brümmer et al., 2005b). On the basis of these results, another field experiment, FRAMZY 2007, was conducted in March and April 2007 with the aim to investigate the impact of cyclones, troughs and fronts on the sea ice in the Fram Strait and to investigate the quality of operational model analyses in representing these phenomena. To this end, a fine-grid net of autonomous buoys was installed on the sea ice and in the open water. Furthermore, research aircraft missions were flown in case of cyclone, trough, or front occurrence in order to measure their three-dimensional structure.

In this paper, we concentrate on the aspect of the quality of the operational model analyses. We use the buoy and aircraft data, which were sampled during FRAMZY 2007 and did not enter into the NWP data assimilation schemes, to estimate the quality of three operational model analyses, the global model of the ECMWF, the global model of the German Weather Service (DWD) and the regional model HIRLAM of the Norwegian Meteorological Institute. In this context, we concentrate on two questions: (a) How good are the SLP analyses? (b) How well is the horizontal and vertical structure in cyclones, troughs and fronts represented? In particular, the second aspect is a challenge for the models since well-mixed and stable boundary layers occur within small distances due to the contrast between open water and sea ice in the Fram Strait.

The paper is organized as follows. The measurements are described in Section 2, the three operational models in Section 3. In Section 4 the results of the SLP comparisons between the buoys and the models are detailed. Section 5 shows the results of the comparisons of the atmospheric boundary layer structure from the aircraft measurements and the models. Summary and conclusions are given in Section 6.

2. Buoy and aircraft measurements during FRAMZY 2007

The FRAMZY 2007 field experiment began on 1 March 2007. Two types of buoys were used; ice buoys of the type CALIB and water buoys of the type XAN-1, both were manufactured by the Canadian company Metocean. The CALIB buoys measured air pressure, temperature and latitude and longitude position, while the XAN-1 buoys measured water temperature (at 0.4 m depth), air pressure, air temperature (at 0.6 m height) and latitude and longitude position. The data were transmitted to satellites of the Argos satellite system by which also the latitude and longitude positions were determined. All buoys were dropped by parachute from a transport aircraft. Due to the large number of buoys, the deployment took place with three flights on 1, 8 and 13 (only XAN-1 buoys) March 2007. Depending on the availability of the Argos satellites the buoy data sequence was between 20 and 90 min. For this study, all buoy data were interpolated to 1-h time resolution. Although XAN-1 buoys have been operated successfully in wintertime Norwegian Sea conditions (Lammert et al., 2008), they worked unreliably with many data gaps during FRAMZY 2007. Thus, only CALIB buoy data are considered here. The measurement duration of the individual buoys was very variable. It depends on how fast they approached the ice edge and were lost there. Here, data from the time interval 1 March through 9 April 2007 are used. The trajectories of the 16 CALIB buoys during this period are displayed in Fig. 1.

For detailed measurements in the atmospheric boundary layer in case of cyclone, trough and front events the German research aircraft Dassault Falcon-20 (referred to as Falcon below) of the German Aerospace Centre in Oberpfaffenhofen was used. The Falcon was equipped with sensors for high-frequency turbulence measurements (sampling rate 100 Hz) of three-dimensional wind

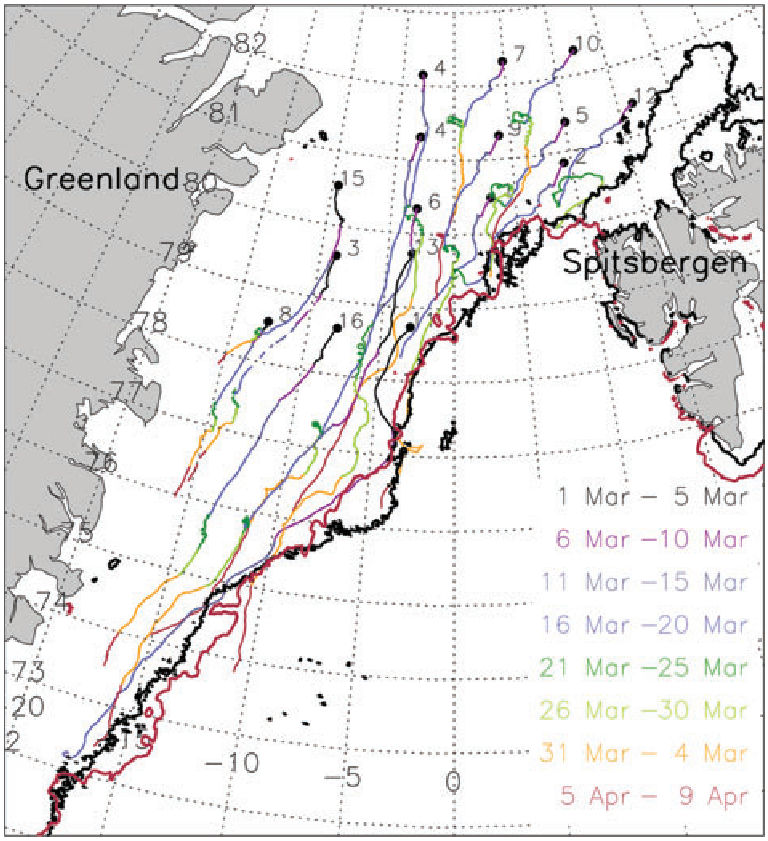

Fig. 1. Drift trajectories of 16 CALIB ice buoys during the period from 1 March to 9 April 2007. Black dots mark the start position. Different colours hold for different 5-d long subperiods. Thick black (red) line represents 20% ice concentration from SSM/I (Special Sensor Microwave Imager) satellite observation on 1 March (9 April).

vector, temperature and humidity. Furthermore, short wave and long-wave up- and downward looking radiometers as well as an infrared sensor for surface temperature, a liquid water content probe, a radio altimeter and a GPS receiver were installed (sampling rate 10 Hz). The Falcon operated from the airfield at Longyearbyen on Spitsbergen. Eight aircraft missions were flown during the period 1–15 March 2007; their locations are shown in Fig. 2. In order to record the three-dimensional structure of the cyclone, trough, or front, the flight pattern consisted of a sequence of low-level runs (30–90 m height depending on the visibility conditions) and vertical profiles. As an example the flight pattern of 5 March 2007 is presented in Fig. 2. Transition time to the experimental area not taken into account, the flight operations in the experimental area lasted 1.5–2 h.

3. The three operational models

The three operational models of the ECMWF, the DWD and the Norwegian Meteorological Institute, whose regular analyses for 00, 06, 12 and 18 UTC are compared with the FRAMZY 2007 measurements in this paper, are briefly described below.

The ECMWF global weather forecast model producing these data from 2007 is a spectral model with T799 resolution. The analysis is generated with a four-dimensional data-assimilation (e.g. Persson and Grazzini, 2005) with a 12-h assimilation window. The resulting fields are available with a horizontal resolution of 0.25° and on 90° vertical levels (15 levels below 1500 m).

The global model of the DWD is an operational weather forecast model on the basis of a triangular grid with 60 km horizontal resolution. The analysis procedure is basically similar to that of the ECMWF model with a 6 h forecast as first-guess field and a three-dimensional optimal interpolation method for data assimilation (e.g. Schrodin, 2002). The data fields are available with a horizontal resolution of 0.5° and on 40° vertical levels (12 levels below 1500 m).

High Resolution Limited Area Model (HIRLAM, see Unden et al., 2002) is a limited-area numerical weather prediction model being developed jointly by several European countries, and is used as operational weather forecast model at several national weather services, among them the Norwegian Meteorological Institute (met.no). It is a regional model on a rotated grid and can be run with various resolutions. Here, we present results from the operational version of met.no in 2007, which was version 6.2.2. It had a horizontal resolution of 0.22° and 40° vertical levels (13 levels below 1500 m). This model uses global forecasts from ECMWF at the lateral boundaries, and is updated with new observations every 6 h using a three-dimensional variational data assimilation system (Gustafsson et al., 2001).

The three models studied differ with respect to the amount of observation data used in the data assimilation. The HIRLAM

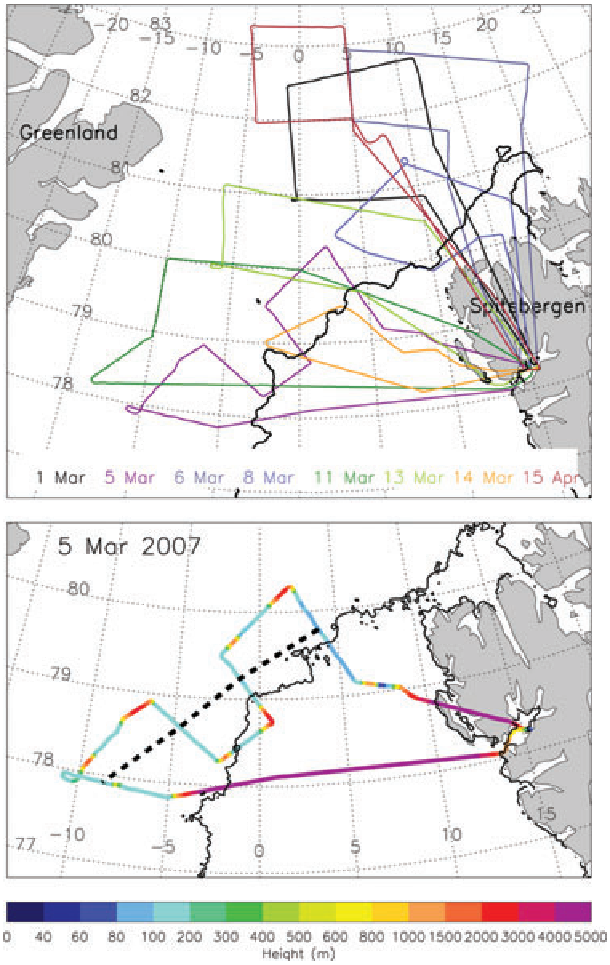

Fig. 2. Top panel: locations of the 8 Falcon flight missions between 1 and 15 March 2007 with 20% SSM/I ice concentration line for 8 March 2007 in the middle of the period. Bottom panel: flight mission on 5 March 2007 through a trough line (dashed; see also Fig. 5) as an example to demonstrate the three-dimensional flight pattern with low-level runs and vertical profiles. Black line is 20% SSM/I ice concentration.

regional model is run with a shorter operational cut-off time than the global models, which means that HIRLAM will miss some observations arriving late which can be used by the other NWP systems. The satellite observation types used by HIRLAM at the time are Advanced Microwave Sounding Unit (AMSU-A) over ocean and scatterometer data. ECMWF used more satellite data, also including more sounding data types, use AMSU over sea ice and use of Atmospheric Motion Vectors (AMVs) from MODIS, which have a good coverage of the Arctic. Some of the differences observed between the model systems will therefore be attributed to theses differences in use of remote sensing data.

The comparisons of the FRAMZY 2007 measurements with the model analyses are performed on the basis of the 6-hourly model time resolution. For the comparison with the buoy data the ECMWF, DWD and HIRLAM SLP fields are interpolated to each buoy position with a distance-weighted average of the next four grid points. For the comparison with the Falcon measurements, which are at various heights, the temperature, humidity and wind fields on each model analysis level are interpolated in space to the individual flight track (virtual flight through the model level data). The comparisons with the Falcon data were only performed for the ECMWF and HIRLAM analyses, since the DWD model level analyses were not available in time.

4. Comparison of sea level pressure based on buoy data

The comparison of SLP is based on the measurements of 16 CALIB buoys in the time interval from 1 March to 9 April 2007, resulting in a total of 2482 6-hourly data (the temporal distribution of the availability of the buoy data is shown in the top panel of Fig. 4).

The scatter diagrams of buoy SLP versus ECMWF, DWD and HIRLAM SLP are presented in the top panels of Fig. 3. For all three models the correlation is higher than 0.99. The mean SLP difference, model minus buoy, is –0.34 hPa for ECMWF, –0.25 hPa for DWD and –0.40 hPa for HIRLAM and the corresponding standard deviations are 0.80, 1.14 and 0.91 hPa, respectively. In the bottom panels of Fig. 3 the SLP tendency within a 6 h time interval is compared. Also, the correlation of SLP tendency is high and amounts to 0.98 for ECMWF, 0.95 for DWD and 0.97 for HIRLAM. The regression line suggests that the magnitude of the SLP tendency is slightly underestimated in all three models. The mean values of the SLP tendency differences are small, as is to be expected and the standard deviations are 0.69 hPa for ECMWF, 1.14 hPa for DWD and 0.91 hPa for HIRLAM.

As a measure of the SLP pattern correspondence, the spatial correlation between the buoy and the model SLP field is calculated for each 6-hourly map. The time series of the spatial correlation is shown in Fig. 4 together with the number of buoys available for the spatial correlation. The spatial correlation averaged over the 40 d long time series from 1 March to 9 April 2007 is 0.98 for ECMWF, 0.94 for DWD and 0.97 for HIRLAM. The time series show a high temporal variation of the spatial correlation. At certain times it drops to values of 0.9 or even lower. For a better understanding of the causes of the spatial correlation changes, the standard deviation of SLP in the array is calculated for the buoy and the model data. Figure 4 shows, that there are only small differences between the SLP standard deviations of buoys and models. Generally, SLP standard deviation is high when a strong pressure gradient is present in the array such as on the side of cyclones or in the region between a low and a high and it is small when a weak pressure gradient is present such as near the centre of a low or high-pressure system. Figure 4 shows that low values of spatial correlation are aligned with low

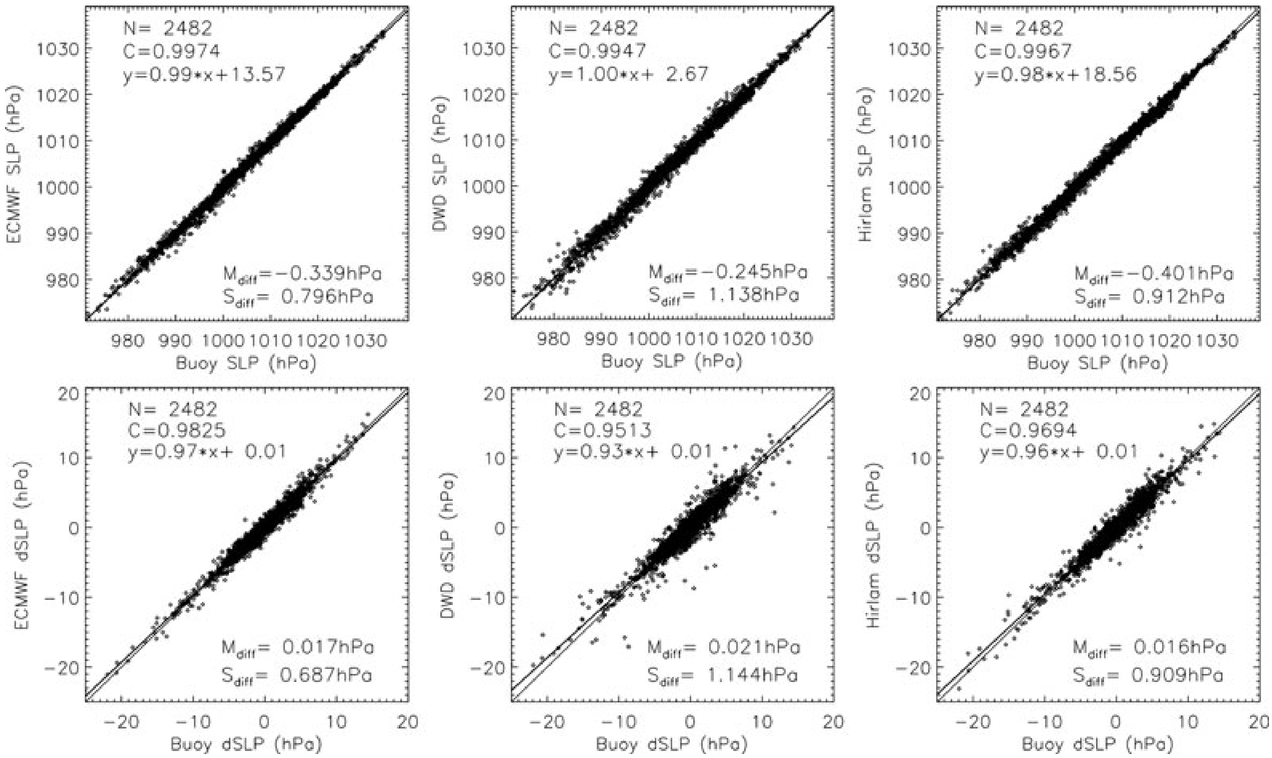

Fig. 3. Upper row: comparison of buoy SLP with model SLP for ECMWF (left-hand panel), DWD (middle panel) and HIRLAM (right-hand panel). Lower row: comparison of SLP tendency within 6 h. Comparisons are based on 6-hourly data pairs ($N = 2482$) for the period 1 March to 9 April 2007. C is correlation coefficient, $y = a\,x + b$ is the regression line, and M_{diff} and S_{diff} are the mean value and the standard deviation of the respective difference.

values of standard deviation. This suggests that in cases of a flat SLP distribution the positions of highs, ridges, lows and troughs are sometimes not placed correctly in the analyses. On the other hand, slight displacements of strong pressure gradient zones may also occur however, they do not lead to a strong reduction of the spatial correlation.

Altogether, statistical SLP comparisons over 40 d in the Fram Strait show some differences between the three operational analyses, but on a high level of agreement with the observational data. This holds for both, the temporal and spatial correlation.

5. Comparison of the atmospheric structure in cyclones, troughs and fronts based on aircraft data

The eight Falcon flight missions took place around or slightly before 12 UTC so that the 12 UTC model analyses of ECMWF and HIRLAM could be used for the comparison of the horizontal and vertical boundary layer structure. Since the comparison results may depend on the complexity of the special synoptic situation, a proper interpretation of the results can only be made with the knowledge of the synoptic situation, which is presented in Section 5.1. The comparison results are detailed in Section 5.2 with respect to the horizontal structure of the SLP and the surface air temperature (SAT), and in Section 5.3 with respect to the vertical structure of temperature, moisture and wind.

5.1. Synoptic situation during the eight flight missions

In Figs. 5, 6 and 7 the SLP and SAT fields of the 12 UTC analyses of the ECMWF model and HIRLAM are presented together with the superposed low-level (30–90 m altitude) aircraft temperature and wind measurements for each flight day. In addition, the 50% ice concentration from the Special Sensor Microwave Imager (SSM/I) satellite observations as well as from the model analysis is given. The ice edge is well represented in both models in the region to the west of 10°E. This does not apply to the observed open water area to the north of Spitsbergen, which is mostly underrepresented in ECMWF model. The prescribed ice concentration in HIRLAM is generally more realistic in this region, although some deviations to the satellite observations occur, too. Tisler et al. (2008) demonstrate the impact of an incorrect ice edge on the atmospheric boundary layer development in case of an on-ice airflow.

On 1 March, a cyclone was present north of Spitsbergen. During the preceding night it has moved from southwest through Fram Strait onto the sea ice. It remained almost stationary in the area of the Falcon flight mission and weakened there. The

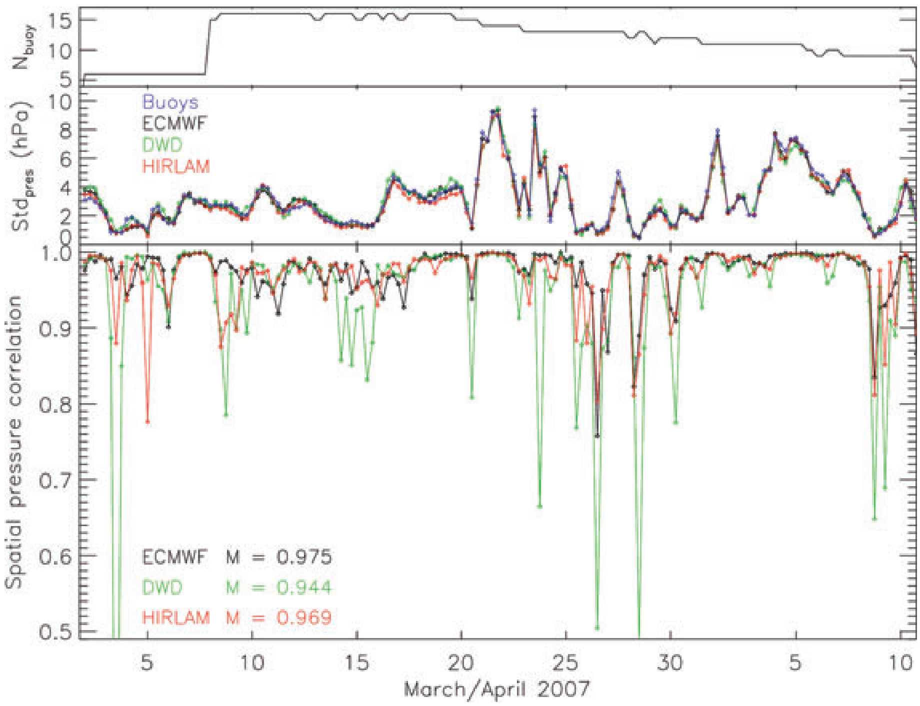

Fig. 4. Top panel: time series of number *N* of available buoys. Middle panel: time series of standard deviation in the SLP fields for buoys, ECMWF, DWD and HIRLAM. Bottom panel: time series of spatial correlation between buoy SLP and model SLP fields for ECMWF, DWD and HIRLAM (together with mean values M).

observed low position is slightly south of the position in both model analyses.

On 5 March, a trough extended from south into the Fram Strait. It progressed further northward and on its eastern side warm air reached the ice edge. This was about the time of the Falcon measurements. In the advancing warm air a weak cyclone developed at the ice edge and moved through the Fram Strait during the following night. It was situated north of Spitsbergen on 6 March and was measured during the third Falcon mission. At this time, the cyclone was already in the decaying stage. The cyclone centre was observed further west than in the model analyses. In this case, the observed vertical structure will be compared in Section 5.3 with the vertical structure of the analysed cyclone, which means a shift of the pattern towards east by 3° in ECMWF and 4° in HIRLAM.

On 8 March, in a generally easterly airflow a trough with an embedded weak low developed at the northwest edge of Spitsbergen. The trough situation remained for an extended period while the low dissolved in the course of the time. Both analyses display the situation rather well.

On 11 March, a trough, which belonged to a low over the Greenland Sea, extended from south into the western part of the Fram Strait. Warm air was transported northward over the sea ice. In the course of the time the trough developed to a low-pressure line with several embedded low-pressure cores, which shifted northward. The flight mission took place in the area between two cores.

The flight mission on 13 March took place on the northwestern side of a weak trough over the eastern part of Fram Strait. This situation remained almost stationary during the flight mission. A strong temperature gradient was not present in the flight area. The measurements on 14 March took place primarily over open water. The aim of the mission was a mesoscale vortex at the ice edge, which was not forecasted but showed up in high-resolution satellite images. In contrast to what could be expected the vortex was weak and dissolving at the time of the flight mission. The ECMWF analysis shows a weak disturbance, the HIRLAM analysis does not.

On 15 March, a cyclone was present north of Spitsbergen. During the preceding night it moved from the Barents Sea along the eastern side of Spitsbergen northward and later northwestward. On its eastern side warm air was transported far to the north leading to an unusual temperature distribution with warm air in the north and cold air in the south. During the time of the flight mission the cyclone was weakening. For this case both model analyses show no more a closed cyclone circulation.

5.2. *Horizontal structure of SLP and SAT*

Table 1 summarizes the results of the comparisons of the horizontal SLP and SAT fields for all eight flight-missions. The comparisons include (a) the representation of the synoptic system in general, (b) the difference in position, (c) the SLP minimum, (d) the maximum SLP difference in the flight area, (e) the

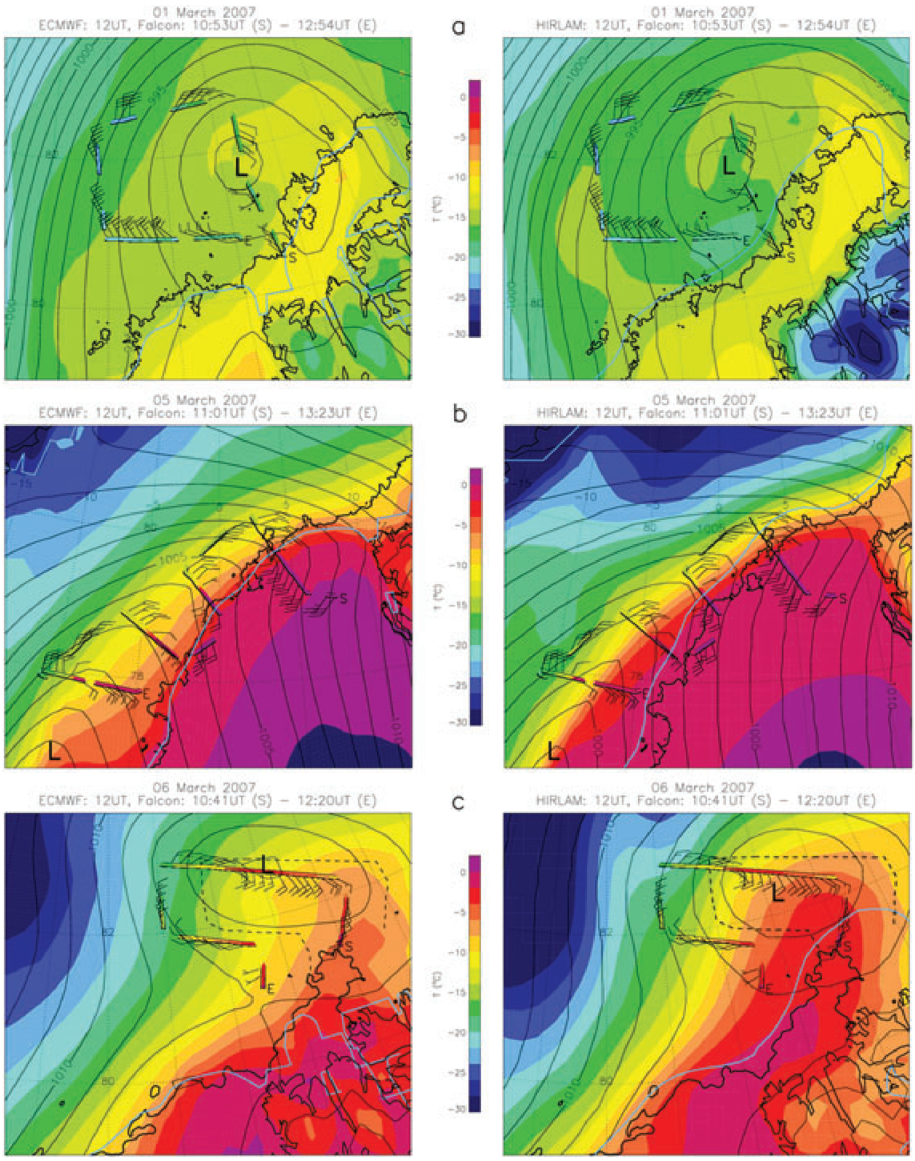

Fig. 5. 12 UTC fields of SLP (thin black lines in 1 hPa intervals) and SAT (colour bars) for ECMWF (left-hand side) and HIRLAM (right-hand side) for the Falcon aircraft fight missions on 1, 5 and 6 March 2007. Falcon low-level (30–90 m) wind and temperature measurements are overlaid. S and E mark start and end positions of the mission. The respective S and E times are given in the header. Thick black (blue) line represents 50% SSM/I (model) ice concentration. The dashed line on 6 March 2007 marks the position at which the model data are taken for the comparison with the aircraft data (see text).

SAT on the warm side and (f) on the cold side of the synoptic system and (g) the maximum SAT gradient in the flight area. The comparisons use only the low-level Falcon flight sections between 30 and 90 m altitude. The air pressure is reduced to sea level; the air temperature is used as measured. The difference between the measured temperature at 30–90 m altitude and the analysed 2 m temperature is estimated as less than 1 K according to the vertical profile flights in Section 5.3.

The synoptic situations are generally well recognized by both models. In nearly all cases, lows, troughs and fronts are well captured. There are only minor differences such as the missing cyclonic disturbance on 14 March in HIRLAM and the untimely low dissolution on 15 March in both models. On 6 March the low position deviates by a distance of more than one model grid point in both analyses. The SLP in the low centre or along the trough shows no systematic deviation, the differences are between –2.1 and +2.6 hPa. These comparison results support those obtained from the buoys, presented in Section 4. Unlike for the SLP are the comparisons for the SLP difference $\Delta p_{Max-Min}$ between the SLP maximum p_{Max} and SLP minimum p_{Min} within the area of the

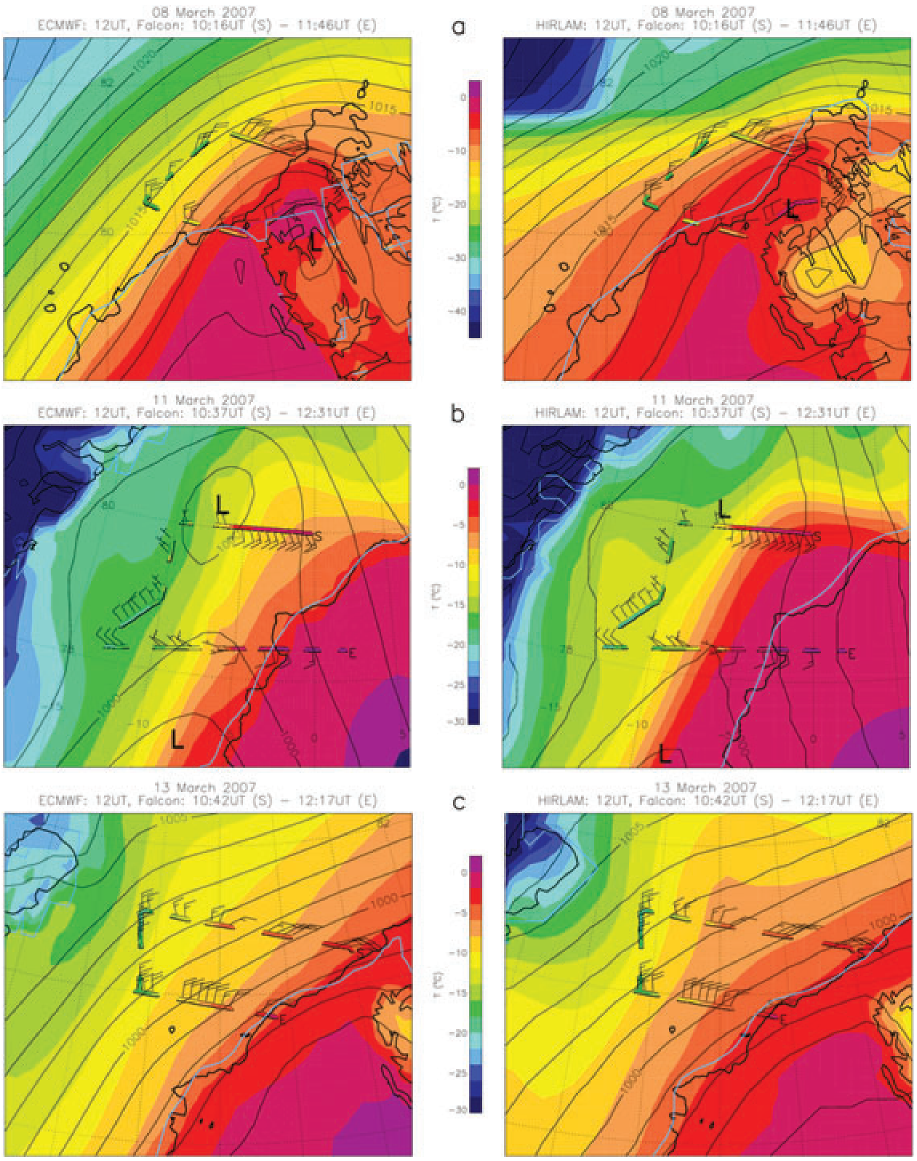

Fig. 6. As Fig. 5, but for 8, 11 and 13 March 2007.

respective flight mission. The observed $\Delta p_{\mathrm{Max-Min}}$ values range from 1.7 to 7.0 hPa. They are systematically underestimated by both model analyses, i.e. the pressure gradient is too small in the vicinity of the low centre or the trough axis. This finding was not possible on the basis of the buoy measurements since they cover all synoptic situations (not only lows, troughs and fronts) and the buoy SLP fields generally have not the necessary small-scale horizontal resolution as the aircraft measurements have.

The comparison of the temperature is distinguished in Table 1 with respect to the warm and cold side of the low or trough. Except for 1 March, the warm-side temperatures were around or slightly below freezing. In these cases the model warm-side temperatures are too low (the maximum difference amounts to –8 K). On 1 March the temperature is generally very low, both on the warm and cold side, and it is overestimated by both models. On the other days, the temperature differences on the cold side show positive as well as negative values (between –4 and +12 K), but with a predominance of positive differences, i.e. the temperatures on the cold side are predominantly too high. Thus, on the average the temperature contrast $\Delta T_{\mathrm{Max-Min}}$ between the maximum temperature T_{Max} and the minimum temperature T_{Min} within the area of the respective flight mission is underestimated in both model analyses (the differences range from -16 to $+3$ K). Comparing the maximum temperature gradient $\Delta T/\Delta x$ within the flight area we obtain a systematic underestimation in all cases and in both models. Averaged over all cases the observed temperature gradient is 2.3 K/10 km. It amounts to 0.8 K/10 km in ECMWF and 0.9 K/10 km in HIRLAM and is thus only one third as large

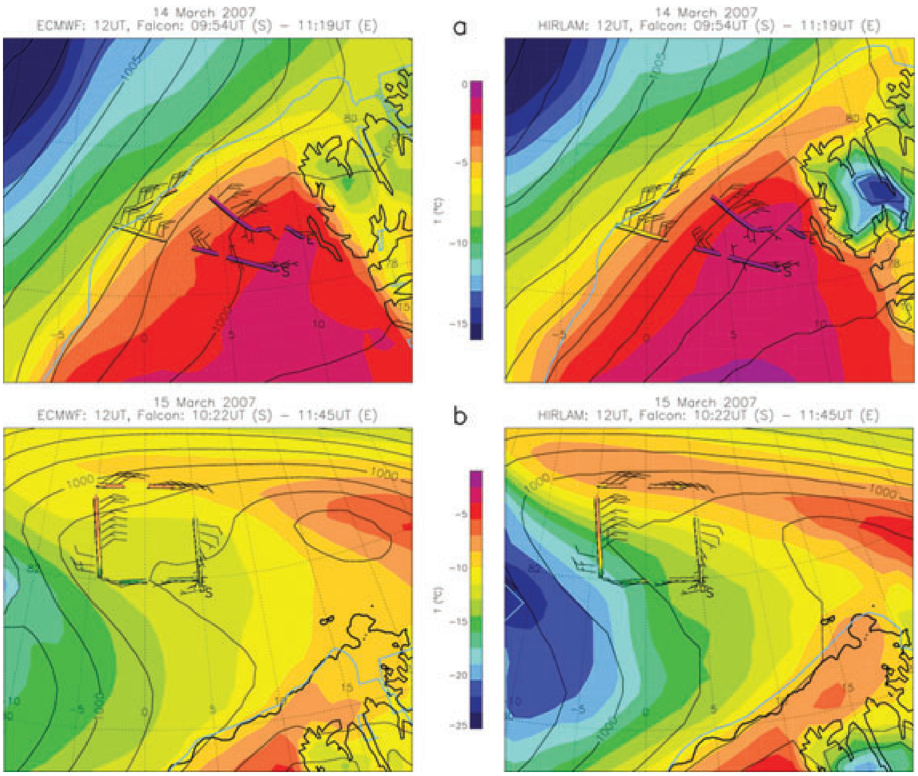

Fig. 7. As Fig. 5, but for 14 and 15 March 2007 (SSM/I ice concentration for 14 March 2007 not available).

as the observed one. Since the observed temperature gradients occurred over distances of 22–110 km, this difference is not only a consequence of the horizontal model mesh width (the shortest resolvable wavelength is 50 km for both models). Furthermore, NWP models usually have some degree of horizontal smoothing through for instance diffusion terms, so that the actual resolution is coarser than the mesh width.

We conclude with respect to the horizontal structure, that the synoptic systems (lows, troughs and fronts) are generally captured but that the horizontal pressure and temperature gradients in the region of the low centre and the trough axis are underestimated in the analyses. This applies both for the ECMWF model and HIRLAM. The differences between both model analyses are small.

5.3. *Vertical structure of temperature, humidity and wind*

The comparison of the vertical structure is based on the aircraft profiles and the corresponding profiles obtained from a virtual flight through the three-dimensional model analysis. The 12 UTC model level analyses of ECMWF and HIRLAM are interpolated to each geographical aircraft position. The observed profiles are interpolated to a regular grid of height versus horizontal flight distance. As an example, the resulting vertical cross-sections (height versus horizontal flight distance) of temperature and wind direction for the flight on 5 March are shown in Fig. 8. During this flight a trough line was crossed four times and profiles were measured both on the warm and cold side. A shallow cold-air layer with northerly winds, which was topped by a sharp inversion, was observed on the cold side. Southerly winds occurred on the warm side as well as above the inversion on the cold side. The models show basically a similar distribution, however, with differences in the vertical and horizontal temperature and wind-direction structure.

This is further detailed in Fig. 9, which shows all temperature profiles (see Fig. 8) both on the warm and cold side from the Falcon observations and the corresponding ones from the ECMWF and HIRLAM analyses. On the warm side a mixed layer was observed and is also modelled with the exception of the lowest few hundred meters where a weakly stable layer is present in the analyses due to the too low SAT as mentioned in Section 5.2. The inversion on the cold side is totally miscaptured in the ECMWF analysis: it is surface-based and too weak. In HIRLAM the observed surface mixed layer and the temperature increase in the inversion are analysed, but the inversion depth is about two times thicker. The temperature differences (model minus Falcon) in the respective right panels of Fig. 9 show a systematically too cold low-level air mass on the warm side of the trough and the non-realistic representation of the inversion on the cold side.

The same classification, i.e. sorting into profiles measured on the warm side and on the cold side of the synoptic system, is

Table 1. Comparison of SLP and SAT from ECMWF (E) and HIRLAM (H) analysis with Falcon (F) low-level measurements for all eight flight missions

	1 March	5 March	6 March	8 March	11 March	13 March	14 March	15 March
Synoptic pattern represented?	Low *N* of Spitsbergen	Warm front trough in FS near ice edge	Low *N* of Spitsbergen	Weak low at NW tip of Spitsbergen	Trough with embedded lows over EGC	Trough over ice in FS	Disturbance at ice edge in FS	Low N of Spitsbergen
in E	Yes	Yes	Yes	Yes	Yes	Yes	Yes	No
in H	Yes	Yes	Yes	Yes	Yes	Yes	No	No
***p*-min**								
Location: F	81.5N,10.0E		82.4N,11.0E	80.0N,13.0E				82.4N,04.5W
Diff.: E-F	50 km	±10 km	50 km	<30 km	∼10 km		<10 km	
H-F	30 km	±10 km	100 km	<30 km	±0 km		No low	
***p*-min**								
F (hPa)	993.4	999.1	1003.9	1012.0	999.9	998.0	999.7	998.5
E-F (hPa)	−1.8	2.6	2.2	−1.1	−0.4	−0.7	0.0	0.2
H-F (hPa)	−2.1	1.4	1.2	−0.9	−0.2	0.5	0.0	0.7
Δp max-min								
F (hPa)	6.2	7.0	3.3	4.4	1.7	6.3	3.4	1.8
E-F (hPa)	−1.3	−2.1	−2.4	−0.1	−0.9	−0.4	−0.1	−0.7
H-F (hPa)	−0.9	−2.7	−2.4	−0.7	−0.7	−1.2	0.4	−1.2
***T* warm side**								
F (°C)	−16	−1/ +1	−3	−1	−3 /−1	−2	−1/0	−7
E-F (K)	2.5	−5/ −3	−4	−2	−8/−6	−2	−1	−3
H-F (K)	1	−1/−2	−2	−3.5	−5/−3	−2/−1	0	−1
***T* cold side**								
F (°C)	−23	−17/ −14	−16	−27	−20	−19	−8	−15
E-F (K)	5.5	0/2	−3	9	3	6 / 7	0	2
H-F (K)	6	1/2	−4	12	5	7/9	1/2	−3
Δ*T* max-min								
F (K)	7	14–16	13	26	18	17	7–8	7
E-F (K)	−3	−3.5	−1	−11	−8	−8	−1	−4
H-F (K)	−5	−2.5	2	−16	−9	−8	−2	3
max *T*-Grad								
F (K/km)	4 K/90 km	11/22	6/30	14/50	10/25	10/60	4/110	7/40
(K/10 km)	0.44	5.0	2.0	2.8	4.0	1.7	0.36	1.75
E (K/km)	2 /130	7/50	8/110	7/70	4/30	4/90	4/100	3/50
(K/10 km)	0.15	1.4	0.7	1.0	1.3	0.44	0.4	0.6
H (K/km)	2/130	7/30	8/90	9/70	8/60	4/120	4/110	4/50
(K/10 km)	0.15	2.3	0.9	1.3	1.3	0.33	0.36	0.8

Notes: Compared are location and value of SLP minimum (*p*-min), SLP difference between maximum and minimum SLP value within the flight area (Δ*p* max-min), SAT on the warm side (*T* warm side) and cold side (*T* cold side) of the synoptic system, SAT difference between the maximum SAT on the warm side and the minimum SAT on the cold side (Δ*T* max-min) as well as maximum SAT gradient given as temperature difference and width of the maximum gradient zone and as gradient in K per 10 km.

applied to all flights. The difference between the analysis and the aircraft measurement is calculated for each profile. Afterwards, the differences are averaged for all profiles on the warm and cold side, separately. The mean observed temperature and wind profiles and the corresponding mean difference profiles (analysis minus Falcon) are displayed in Figs. 10 and 11 for the warm side and the cold side of the synoptic system, respectively. The wind profiles are presented in a rotated coordinate system (index *R*) in which the u_R (v_R) wind component is parallel (normal) to the observed wind direction in the lowest 100 m. The same reference wind direction is used for all profiles of the same class and for both the measurements and the analyses. The reference wind directions are listed in Figs 10 and 11. The use of the rotated compared to the normal geographic coordinate system allows an

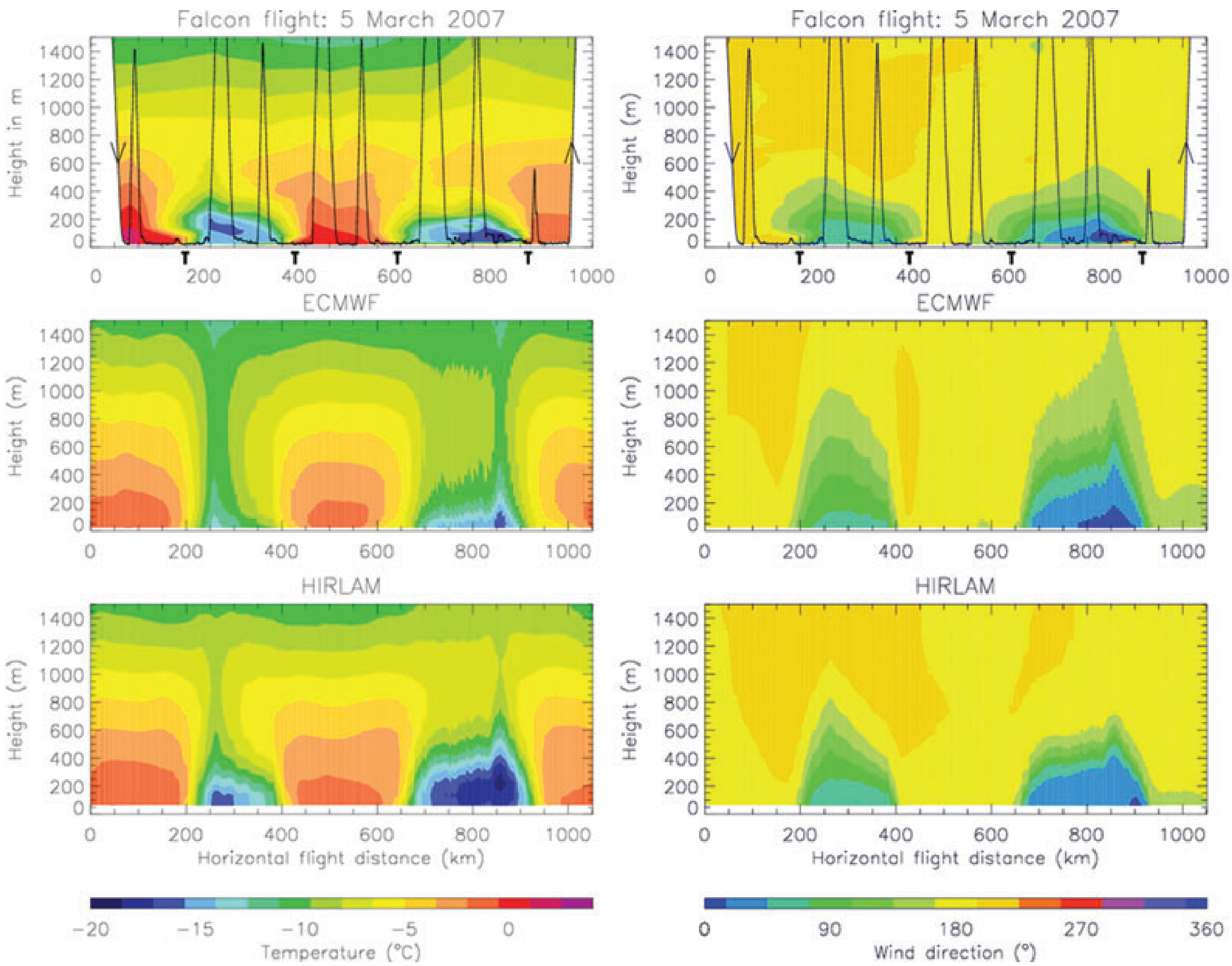

Fig. 8. Vertical cross-section (height versus horizontal flight distance) of air temperature (left-hand panel) and wind direction (right-hand panel) from Falcon aircraft measurements (top panel) and ECMWF (middle panel) and HIRLAM (bottom panel) analysis for the flight mission on 5 March 2007 with four intersections of a trough line (T). Thin black line marks Falcon flight pattern (see also Fig. 2 and Fig. 5b).

easier comparison of the results obtained under eight different synoptic conditions.

On the warm side of the synoptic systems (Fig. 10), the observed temperature stratification in the lowest 500 m was between neutral (1, 5 and 14 March), near isothermal (8, 13 and 15 March) and a weak inversion (6 and 11 March). The parallel wind component u_R increased with height on most days and even exhibited a low-level jet on 4 d (6, 8, 13 and 15 March). The normal wind component v_R decreased with height as should be expected due to frictional veering and warm air advection. The wind profiles on 1 and 14 March deviate from the others with much less wind shear in both components due to the weak thermal stratification. Both model analyses underestimate the air temperature by 1–4 K in the lowest 900 m on all days except for 1 March when the air was rather cold even on the warm side of the cyclone. The u_R wind component is generally too small by 1–5 m s^{-1} in the lowest 300 m in both model analyses. The v_R component is predominantly too large by 0–4 m s^{-1} in the HIRLAM analysis and deviates by ±2 m/s in the ECMWF analysis. This means that the analysed low-level wind on the warm side of the synoptic systems is predominantly too small and, in case of the HIRLAM analysis, is directed more than observed towards low pressure. The general wind bias in the analyses appears to be a consequence of the underestimated low-level air temperature and, thus, overestimated stability in the boundary layer.

On the cold side of the synoptic systems (Fig. 11) a shallow cold-air layer with a depth of less than 200 m, which was topped by an inversion with a temperature increase of 3–15 K was observed on most days. Only on 1 March when the wind was considerably stronger than on the other days the cold-air layer had a depth of about 500 m. Above the inversion, the temperature on the cold side approached that on the warm side indicating that the observed lows and troughs over the sea ice were predominantly low-level phenomena. The parallel wind component u_R increased slightly with height within the shallow cold-air

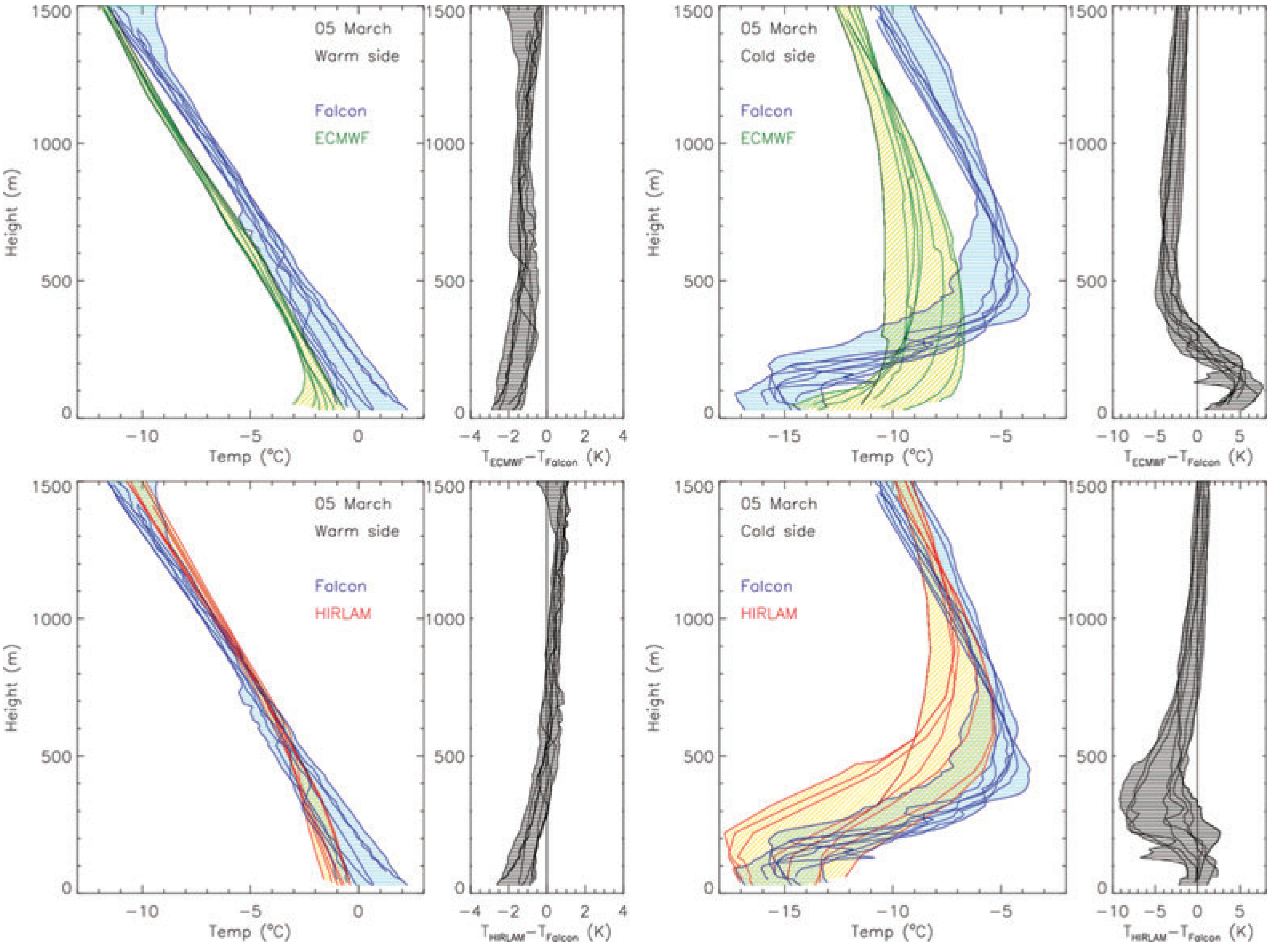

Fig. 9. Temperature profiles from Falcon aircraft measurements (blue) and ECMWF (green, top panel) and HIRLAM (red, bottom panel) analysis together with the corresponding differences (grey) on the warm side (left-hand panel) and cold side (right-hand panel) of the trough line on 5 March 2007.

layer and decreased, on some days even strongly, within the inversion layer, thus, resulting in a weak low-level wind maximum. The normal wind component v_R decreased slightly with height in the cold-air layer but strongly in the overlying inversion. Thus, there was a strong wind shear together with a strong veering of the wind in the inversion layer on the cold side of most synoptic systems. Both model analyses are not able to represent the sharpness and the strength of the inversion. In most cases, the cold-air layer is too warm and the inversion layer too cold, in the same way as was shown in Fig. 9. Thus, the analysed stability in the inversion is weaker than observed. The u_R wind component in the cold-air layer is predominantly too small in the analyses. The same holds for the v_R component, particularly in the ECMWF analysis. In the inversion layer and further above, wind deviations are partly large but show no systematic bias as in the cold-air layer. The systematically too small values of u_R and v_R in the model analyses mean that the analysed wind in the cold-air layer is turned too much to the right towards the direction of the upper-level wind. This may be a consequence of vertical stability within the inversion and, thus, leads to an overestimation of the vertical mixing between the momentum in the cold-air layer and the inversion layer.

We can summarize the results of the profile comparisons on the warm and cold side of the cyclones and troughs as follows. The boundary-layer air on the warm side is too warm and too stable stratified and, thus, the wind is too weak and directed too much towards the low pressure in the model analyses. On the cold side, the boundary layer air is too warm and the overlying inversion is too weak. The reduced vertical stability allows a higher degree of coupling between the boundary-layer wind and the upper-level wind and, thus, leads to a boundary-layer wind, which is directed too much towards the high pressure.

The deficits in the temperature representation in the model analyses appear to be the reason for the wind deficits. It should be mentioned that we also compared the specific humidity and found that the humidity differences between the analyses and the observation have a vertical distribution, which is very similar to that of the temperature differences.

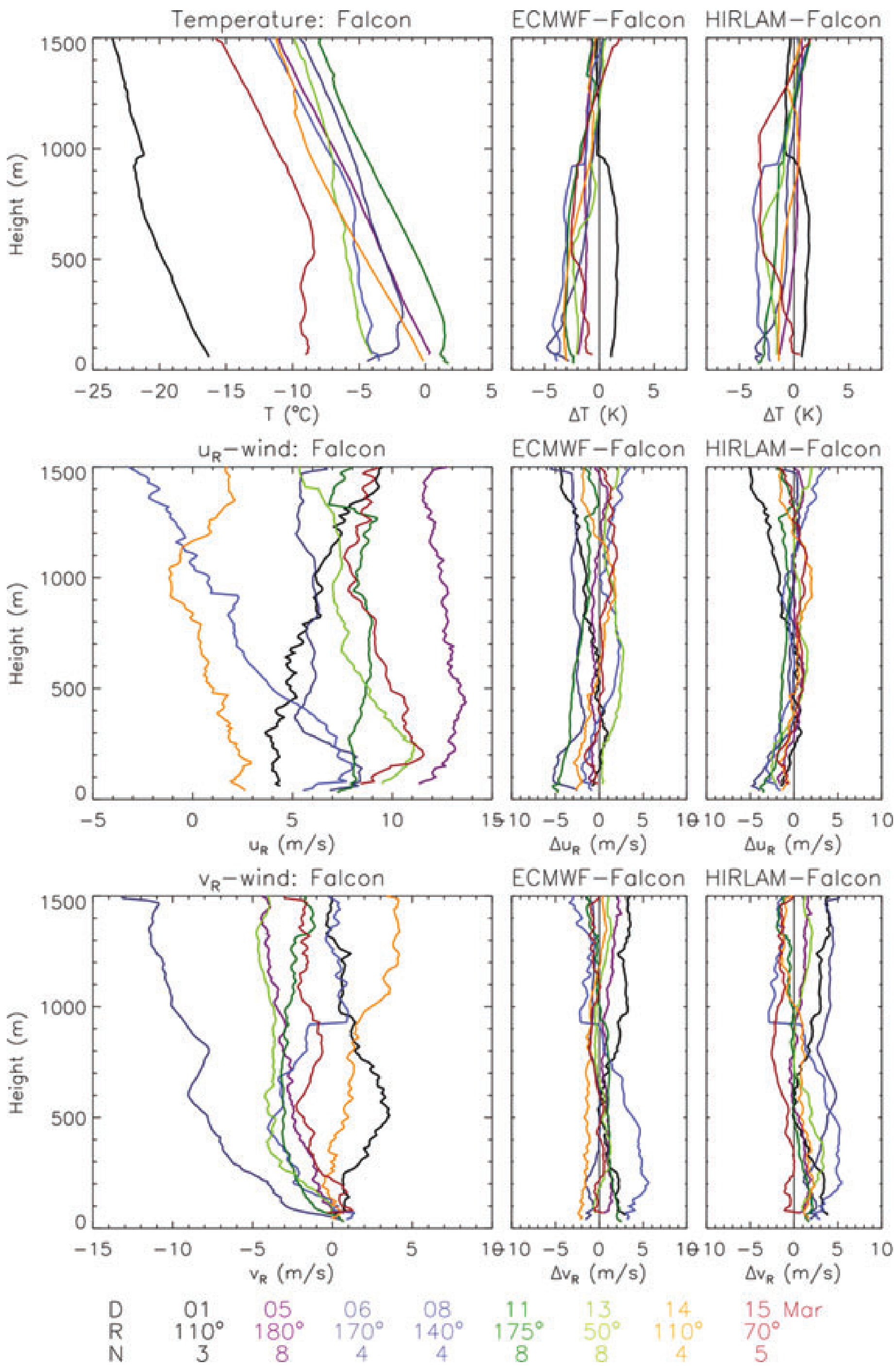

Fig. 10. Vertical profiles on the warm side of the eight synoptic systems: mean measured temperature (top panel), parallel u_R (middle panel) and normal v_R (bottom panel) wind component together with the corresponding mean differences (analysis minus Falcon aircraft). The reference wind directions (R) used for the rotated wind components as well as the number of profiles (N) available for the calculation of the means are listed below.

The temperature differences between measurements and model analyses hint at two problems in the models: (a) the first issue is the low-level cold bias on the warm side and the warm bias on the cold side. This hints at deficits in the representation of the surface temperature and, thus, the surface energy balance, which in turn may result from erroneous surface properties (snow and ice thickness, heat conduction, etc.) or a faulty radiation balance (up- and downwelling radiation fluxes, albedo, clouds, etc.). (b) The second issue is the representation of the inversion in the cold air. This deficit appears to be closely

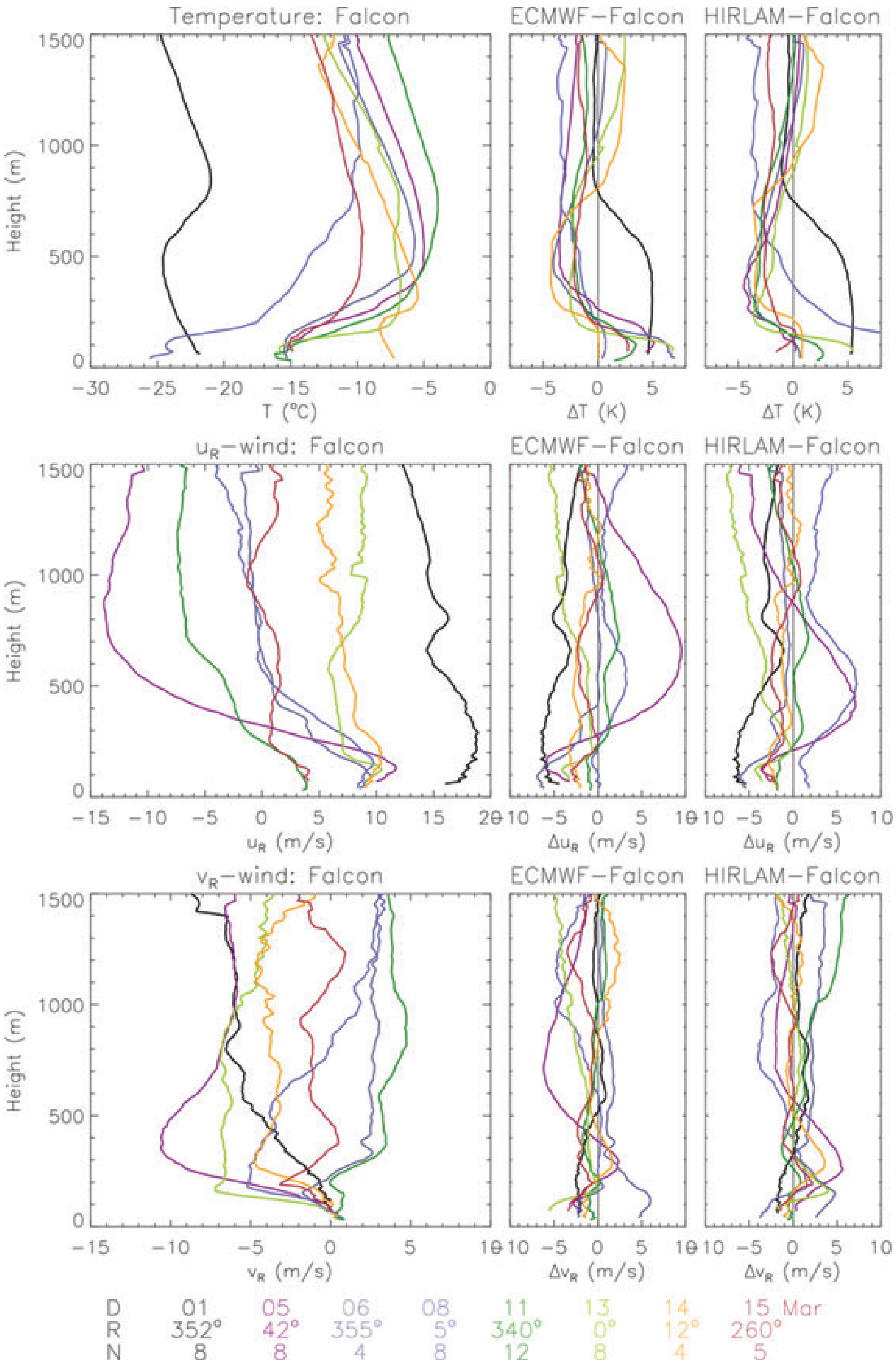

Fig. 11. As Fig. 10, but for the cold side of the synoptic systems.

connected to the parametrization of the vertical mixing and its dependence on the stability.

6. Summary and conclusions

In this paper, the operational analyses of three NWP models (ECMWF model, DWD model and HIRLAM) are compared to observations performed by 16 ice buoys and the research aircraft Falcon during the FRAMZY field experiment in the Fram Strait in March and April 2007.

The comparison of the SLP between the buoys and the model analyses is based on 2482 6-hourly data and shows a generally good agreement. The correlations for the SLP are higher than 0.99 and the correlations for the 6-hourly SLP tendencies are between 0.95 and 0.98. The spatial correlations for the SLP fields on the average are between 0.94 and 0.97 and are only smaller when a synoptic system, high/ridge or low/trough, is in the buoy array and when its position in the analysis is slightly displaced. Concerning the SLP comparison the differences between the three models are small.

The comparison of the horizontal and vertical boundary layer structure is based on eight aircraft flights through Fram Strait cyclones, troughs and fronts predominantly over the sea ice. These comparisons are performed for the ECMWF and HIRLAM model analyses. Nearly all synoptic systems are captured by the models with only small deviations concerning their positions and the SLP in the cyclone core or along the trough line. Concerning the horizontal structure the SLP gradient between the low/trough centre and the surrounding is slightly underestimated and the SAT is too cold on the warm side and too warm on the cold side. This leads to too small SAT contrasts across the respective synoptic system in both models. Furthermore, the SAT contrast is distributed over a too large distance. On the average, the maximum horizontal SAT gradient in the models is only one third as strong as observed. This underestimation appears to be no consequence of the model grid resolution. Concerning the horizontal SAT gradient the HIRLAM analysis is slightly better than the ECMWF analysis.

The vertical structure of temperature and wind is compared for the warm and the cold side of the low/trough system. The cold SAT bias on the warm side of the system effects the lowest several 100 m, the low-level stratification is too stable. On the cold side of the system the temperature inversion is not realistically captured with respect to its base and strength in the ECMWF analysis and with respect to the vertical thickness in the HIRLAM analysis. The deficits in the representation of the vertical stratification directly influence the vertical structure of humidity and wind. Altogether, the vertical structure is better represented in HIRLAM than in ECMWF. The errors in SAT indicate deficits in the simulation of the surface temperature of snow and ice while the errors in the inversion analysis hint at deficits in the parametrization of the vertical mixing.

As mentioned above, the SLP analyses capture nearly all significant synoptic systems. Thus, the SLP fields appear to be an acceptable database for climate statistics (e.g. cyclone frequencies). Also, using the model SLP analyses, as dynamic forcing in an ice or ice-ocean model appears to be reasonable. For the overall good quality of the SLP analysis, the use of drifting buoys in the Arctic (e.g. the buoys from International Arctic Buoy Programme, IABP) plays an important role as was demonstrated by Inoue et al. (2009). Remember that our FRAMZY 2007 buoy and aircraft data did not enter into the NWP systems.

The same conclusion concerning the model analysis quality cannot be drawn with respect to the SAT analysis. If the SAT analyses are used as thermodynamic forcing of a sea ice model, systematic temperature deviations as identified in this analysis may lead to systematic errors in the heat budget of the sea ice.

The consequences of the supposed model deficits behind the systematic errors found in the analyses of the SAT and the temperature inversion over sea ice are presumably small for the short-range weather prediction. However, the deficits probably lead to growing errors and limit the quality of extended weather forecasts for the ice-covered polar areas. Furthermore, many climate models are based on NWP models and use the same surface temperature models and vertical mixing parametrizations. The consequences of such systematic deficits in a climate model are much more severe.

7. Acknowledgments

This research was funded by the German Science Foundation (DFG) under grant SFB 512 ‘Cyclones and the North Atlantic Climate System’.

References

Affeld, B. 2003. *Cyclones in the Arctic and Their Impact on the Sea-Ice Transport trough the Fram Strait (In German)*. PhD Thesis, Univ. Hamburg.

Brümmer, B. (ed.) 2000. Field Experiment FRAMZY 1999—cyclones over Fram Strait and their impact on sea ice: field report with examples of measurements. *Ber. Zentrum für Meeres- und Klimaforschung, Reihe A*, No. 33, pp. 176, Univ. Hamburg.

Brümmer, B., Thiemann S. and Kirchgäßner A. 2000. A cyclone statistics for the Arctic based on European Centre re-analysis data. *Met. Atmos. Phys.* **75**(3–4), 233–250.

Brümmer, B., Müller, G., Affeld, B., Gerdes, R., Karcher, M. and co-authors. 2001. Cyclones over Fram Strait: impact on sea ice and variability. *Polar Res.*, **20**, 147–152.

Brümmer, B., Launiainen, J., Müller, G. and Schröder, D. 2005a. Field Experiment FRAMZY 2002—second experiment on cyclones over Fram Strait and their impact on sea ice: field report with examples of measurements. *Ber. Zentrum für Meeres- und Klimaforschung, Reihe A*, No.37, pp. 154, Univ. Hamburg.

Brümmer, B., Müller, G. and Schröder, D. 2005b. In-situ observations in cyclones over Fram Strait. *Meteorol. Z.* **14**(6), 721–734.

Brümmer, B., Schröder, D., Müller, G., Spreen, G., Jahnke-Bornemann, A. and co-authors. 2008. Impact of a Fram Strait cyclone on ice edge, drift, divergence and concentration: possibilities and limits of an observational analysis. *J. Geophys. Res.* **113**, C12003, doi: 10.1029/2007JC004149.

Gustafsson, N., Berre, L., Hörnquist, S., Huang, X.-Y., Lindskog, M. and co-authors. 2001. Three-dimensional variational data assimilation for a limited area model. Part I: general formulation and the background error constraint. *Tellus* **53A**, 425–446.

Häkkinen, S. 1993. An Arctic source for the Great Salinity Anomaly: a simulation of the Arctic ice-ocean system for 1955–1975. *J. Geophys. Res.* **98**, 16397–16410.

Häkkinen S. and Geiger, C. A. 2000. Simulated low frequency modes of circulation in the Arctic Ocean. *J. Geophys. Res.* **105**, 6549–6564.

Harder, M., Lemke, P. and Hilmer, M. 1998. Simulation of sea ice transport through Fram Strait: natural variability and sensitivity to forcing. *J. Geophys. Res.*, **103**, 5595–5606.

Hilmer, M., Harder, M. and Lemke, P. 1998. Sea ice transport: a highly variable link between Arctic and North Atlantic. *Geophys. Res. Lett.* **25**, 3359–3362.

Hilmer, M. and Jung, T. 2000. Evidence for a recent change in the link between the North Atlantic Oscillation and Arctic sea ice export. *Geophys. Res. Lett.* **27**, 989–992.

Inoue, J., Enomoto, T., Miyoshi, T. and Yamane, S. 2009. Impact of observations from Arctic drifting buoys on the reanalysis of surface fields. *Geophys. Res. Lett.* **36**, L08501, doi:10.1029/2009GL037380.

Jahnke-Bornemann, A. and Brümmer, B. 2009. The Iceland—Lofotes pressure difference: different states of the North Atlantic low-pressure zone. *Tellus* **61A**, 466–475.

Kwok, R. and Rothrock, D. A. 1999. Variability of Fram Strait ice flux and North Atlantic Oscillation. *J. Geophys. Res.* **104**, 5177–5189.

Lammert, A., Brümmer, B., Ebbers, I. and Müller, G. 2008. Validation of ECMWF and DWD model analyses with buoy measurements over the Norwegian Sea. *Met. Atmos. Phys.* **102**, 87–96.

Persson, A. and Grazzini, F. 2005. User guide to ECMWF forecast products. Technical Report Meteorological Bulletin M3.2, European Centre for Medium-Range Weather Forecast.

Polyakov, I. V. and Johnson, M. A. 2000. Arctic decadal and interdecadal variability. *Geophys. Res. Lett.* **27**, 4097–4100.

Proshutinsky, A. Y. and Johnson, M. A. 1997. Two circulation regimes of the wind-driven Arctic Ocean. *J. Geophys. Res.* **102**, 12493–12514.

Schröder, D. 2004. *Cyclone Impact on Sea Ice in the Fram Strait: Modelling and Observations (In German)*. PhD Thesis, Univ. Hamburg.

Schrodin, R. 2002. Quarterly Report of the German NWP System. Technical Report Part 2: Description of the German NWP System, German Weather Service. Available at http://www.dwd.de/en/FundE/Veroeffentlichung/Quarterly_new/Quartely_new.htm.

Serreze, M. C. 1995. Climatological aspects of cyclone development and decay in the Arctic. *Atmos. Oceans* **33**, 1–23.

Tisler, P., Vihma, T., Müller G. and Brümmer, B. 2008. Modelling of warm-air advection over Arctic sea ice. *Tellus* **60A**, 775–788.

Undén, P., Rontu, L., Järvinen, H., Lynch, P., Calvo, J. and co-authors. 2002. HIRLAM-5 Scientific Documentation, December 2002. Available at www.hirlam.org.

Vinje, T. 2001. Fram Strait ice fluxes and atmospheric circulation: 1950–2000. *J. Clim.* **14**, 3508–3517.

Zhang, Y., Walsh, J. E., Zhang, J., Bhatt, U. S. and Ikeda, M. 2004. Climatology and interannual variability of Arctic cyclone activity: 1948–2002. *J. Clim.* **17**, 2300–2317.